Materials Science and Engineering B 310 (2024) 117759

Contents lists available at ScienceDirect

Materials Science & Engineering B

journal homepage: www.elsevier.com/locate/mseb

3D printed $CuZnAl_2O_3$-based catalysts for direct CO_2 hydrogenation to DME, optimization and scale up

Yoran De Vos [a], Arie J.J. Koekkoek [b], Giuseppe Bonura [c], Serena Todaro [c], Monika Kus [a], Alexander Vansant [a], Gijsbert Gerritsen [b], Catia Cannilla [c], Hendrikus C.L. Abbenhuis [b], Vesna Middelkoop [a,*]

[a] Materials and Chemistry (MatCh), Flemish Institute for Technological Research, VITO NV, Boeretang 200, 2400 Mol, Belgium
[b] HYBRID CATALYSIS, Den Dolech 2, 5612 AZ Eindhoven, Netherlands
[c] CNR-ITAE, Istituto di Tecnologie Avanzate per l'Energia "Nicola Giordano", Via S. Lucia sopra Contesse 5, 98126 Messina, Italy

ARTICLE INFO

Keywords:
CO_2 hydrogenation
DME
Methanol
Binary catalytic system
3D printing

ABSTRACT

This work reports the development, optimization and subsequent scale-up of 3D printed catalyst structures for direct CO_2 hydrogenation to DME. To ensure compatibility between the used Cu-ZnO-Al_2O_3 (CZA) catalyst and the acid form H-ZSM-5 co-catalyst, a new binary polymeric binder system, based on polyethyleneimine (PEI) and methylcellulose (MC), was selected. The 3D-printing paste composition was optimized through 2 successive Design of Experiments (DOE) to achieve (i) good textural properties that ensure catalytic activity and (ii) improved mechanical integrity and printability. The DOE unveiled the critical link between the pH of the printing paste and the preservation of textural properties and catalytical activity of the printed catalysts. Finally, the successful scale-up of the 3D-printed catalyst structures was demonstrated using the optimized printing paste, and the performance of the final catalysts was evaluated by catalytic testing and accompanied X-ray Diffraction (XRD), Scanning Electron Microscopy (SEM) and Energy Dispersive Spectroscopy (EDS) analyses.

1. Introduction

Carbon Capture and Utilization (CCU) technologies employ captured CO_2 that is typically recycled into other components and products, such as chemical feedstocks, fuels or building materials, which would otherwise be derived from fossil-based resources [1,2,3]. The work presented herein was conducted as part of the EU Horizon CO2Fokus project, aiming to develop an innovative reactor design for direct dimethyl ether (DME) production from H_2 and CO_2 as feedstock instead of syngas. To this end, a multi-phase catalyst system was employed, comprising Cu-ZnO-Al_2O_3 (CZA) and ZSM-5 zeolite. The overall goal was to deliver a sustainable, energy efficient and economically viable process to convert green H_2 and industrial CO_2 into DME, with huge potential for avoiding emissions in the atmosphere from energy intensive industries [4,5,6].

To tackle the technological challenges behind current chemical conversion technologies, new catalytic, high-performance materials were developed using innovative 3D printing technology. Conventional catalyst shaping techniques, such as extrusion and pelletizing, have limitations. The catalyst is often not efficiently used, because reactants cannot reach the active sites inside the pellet. The pellets cannot be made smaller as that can lead to an increase in the pressure drop [7,8]. Other well-known structured catalyst shapes are monolithic/honeycomb structures alongside catalytic foams. Foam structures show good radial heat and mass transfer, adjustable pressure drop, but they lack a precise control of the flow due to the more random porous structure [9]. The monolith or honeycomb reactors are commercially used as reactor configurations in the fuel reforming industry. They make use of arrays of parallel passageways for directed gas flows [10]. The active catalyst material is commonly coated on the channel walls of the solid monolith/honeycombs [11]. Previous reports have already shown commercially available Cu/ZnO/Al_2O_3 catalyst, wash coated on metal open-cell foams and monoliths, as promising for the intensification of the methanol synthesis [12,13].

3D printing has recently taken off as a technical advancement in mimicking monoliths/honeycombs, allowing for the direct patterning of (multichannel) catalyst reactors with active materials and supports of choice [14,15,16,17]. A comparison of 3D printed monoliths and

* Corresponding author.
E-mail address: vesna.middelkoop@vito.be (V. Middelkoop).

https://doi.org/10.1016/j.mseb.2024.117759
Received 15 July 2024; Received in revised form 6 October 2024; Accepted 9 October 2024
Available online 26 October 2024

conventional packed bed reactors has shown that the former can offer superior performance due to high geometric surface area, high mass transfer rates and easier scale-up [18,19]. 3D printed structures offer superior tunability and reproducibility of physico-chemical properties of materials. This results in a high geometric surface area, high mass transfer rates, reducing pressure drop in the reactor and allowing reagents to reach the entire catalyst. Furthermore, they enable easy scale-up and product-catalyst separation, which has a direct effect on the sustainability and cost of the process [20].

There are quite a few different 3D printing technologies, such as Fused Deposition Modelling (FDM), Stereolithography (SLA), Digital Light Processing (DLP), Selective Laser Sintering (SLS) and Selective Laser Melting (SLM) (as previously described in the literature) [21,22,23,24,25,26]. However, Micro Extrusion, also known as Direct Ink Writing (DIW), has been used most frequently for applications where porous materials are needed, such as catalysis and adsorption. As typically in any composites processing technology, DIW relies on high solid contents i.e., highly concentrated suspensions of particles and it is essential to control the rheological properties of these suspensions [27,28]. The design of the suspensions (inks) represents the most critical aspect of DIW. An adequate ink requires an appropriate solid loading and rheological (shear thinning) properties tuned to allow for extrusion and ensure the necessary fidelity and structural stability of the final shaped material [29]. For applications such as catalysis and adsorption, it is important to preserve the surface properties of the catalytic materials and adsorbents, to ensure catalytic/adsorption activity. This adds an extra layer of complexity to the whole process, as it may limit the working window of the printing process, and post-printing treatment, such as the calcination temperature.

This work presents the successful development, optimization and subsequent scale-up of 3D printed mixed phase CZA-ZSM-5 catalyst for direct CO_2 hydrogenation to DME, building on the authors recent work [30]. We highlight the importance of the effect of the printing paste composition on the rheological properties and final structural stability of the printed materials, as well as the effect on the textural properties that are needed for the final application. This multi-factorial multi-disciplinary problem is addressed efficiently using Design of Experiments. Finally, the successful scale-up of the 3D-printed catalyst structures is demonstrated using the optimized printing paste. The performance of the final catalysts is evaluated in a single-tube catalytic reactor.

2. Experimental

2.1. Starting formulations – reference systems

Materials used to prepare the 3D printed catalysts include a commercial Cu-ZnO-Al_2O_3 catalyst i.e. CZA (supplied by Alfa Aesar) and ZSM-5. The starting powders, CZA and ZSM-5, were combined at a constant weight ratio of 1:1 between the metal-oxide catalyst and the zeolite co-catalyst. Before mixing, ammonium-ZSM-5 (supplied by Alfa Aesar, $SiO_2/Al_2O_3 = 23.1$) was calcined at 500 °C for 4 h to obtain the acid form H-ZSM-5.

2.2. 3D-printing

The CZA-based systems were developed by printing the solid powder coming from the mechanical mixing of the metal-oxide(s) phase and acid zeolite phase (in a weight ratio 1:1). Prior to printing, each powder was suspended into a polymer solution of polyethyleneimine (PEI) and methylcellulose (MC) to obtain a printing ink/paste. The paste included a certain fraction (wt.%) of an alumina based inorganic binder (Disperal P2, Sasol) with the final catalyst dry content amounting to up to 90 wt%. A series of structures were 3D printed by micro-extrusion (fibre deposition, also referred to as direct ink writing) through a thin nozzle depositing the material in a layer-by-layer fashion. The final geometries, whether in cuboid or cylindric form were dried and subsequently calcined at 500 °C.

2.3. Paste characterization

Before printing, the pH of the printing pastes was measured using a Mettler Toledo SevenCompact Duo pH meter using with an InLab Expert Pro ISM probe.

The rheological behaviour of the pastes plays a key role in the development of 3D printed catalysts. This behaviour was evaluated using a Haake Mars 60 Rheometer at 25 °C, using a plate-plate configuration with a 35 mm Ti plate and a gap of 1 mm. To avoid the drying of the printing pastes during the measurement, a two-part polyoxymethylene sample hood with an integrated inner and outer solvent trap was used, containing demineralised water. The pastes were applied to the plate; after reaching the gap height, the pastes were equilibrated for 1 min before starting the oscillation measurement. The oscillation measurements (stress-controlled amplitude sweep) were started at a shear stress of 7.5 Pa up to 10^4 Pa with a break criterium when the displacement angle exceeded 0.4 rad to avoid excessive paste removal from between the plates.

2.4. Material characterization

The zeta potential of the catalyst powders was executed with a colloidal dynamics Zeta probe analyzer with a flow-through cell. Typically, 5 wt% suspensions in an ionic buffer of 10 mM KCl solution in demineralised water were made.

To characterize the phase composition of the catalyst powders and printed catalysts, powder X-ray diffraction (XRD) experiments were performed using a Philips X'Pert diffractometer with PANalytical X'Pert Pro software with CuKα ($\lambda = 1.5405$ Å) at 40 kV. The printed catalysts were investigated by Scanning Electron Microscopy (SEM) using a FEI NOVA NanoSEM 450 with an Energy Dispersive Spectroscopy (EDS) system.

2.5. Catalytic tests

The printed monolithic catalyst was finally tested for its performance for CO_2 reduction to DME. In two separate experiments, one monolith (4.35 g) and two stacked monoliths (9.55 g) respectively were introduced in a 1″ reactor inside an electrical furnace. The small space between the printed monolith and the inside wall of the reactor (1 mm) was filled up with 40 μm sized SiC. Initial tests on the single and double monoliths were executed using a feed of 0.82 SLM and a H_2: CO_2 ratio of ~4 (0.62 SLM H2, 0.15 SLM CO_2 and 0.05 SLM Ar, where SLM denotes standard liters per min) at 29.7 barg. A standard temperature sweep was applied up to 290 °C (x°C/min) after which the reactor was set to 265 °C for a duration test for 17 h for the single monolith reactor and 60 h for the stacked monolith reactor.

3. Results and discussion

3.1. 3D printing paste formulation for the catalysts for CO_2 conversion to DME

As initial printing pastes (not included in the publication) displayed issues related to instability and nozzle clogging, Zeta potential measurements were carried out on the main constituents of the catalyst printing paste (the mixed oxide and the zeolite). The measurements established the magnitude and 'sign' of the charge at the surface of particles inside a medium. Particles with zeta potentials that are more positive than +30 mV or more negative than −30 mV are generally regarded as being in a 'stable' state in a suspension. This approach is probably not directly transferrable to printing pastes due to the much higher solids content when compared to conventional suspensions, but can still give an indication of the pH region where attractive interactions

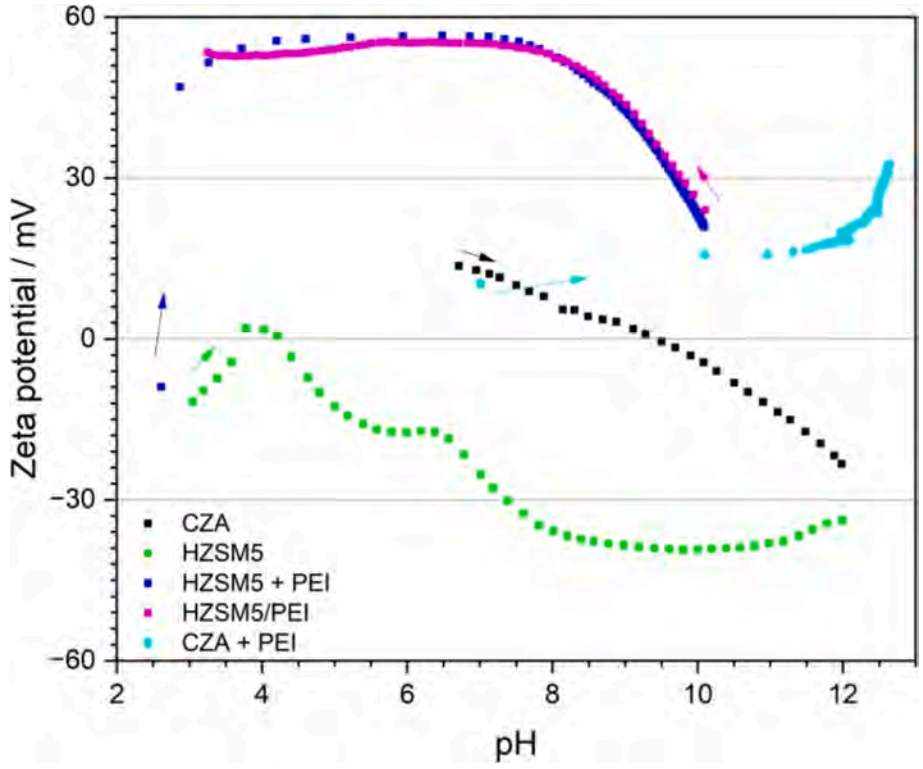

Fig. 1. Zeta potential measurements on catalyst (CZA) and co-catalyst (H-ZSM-5) powders and the effect of PEI addition to the 3D printing paste on their zeta-potential.

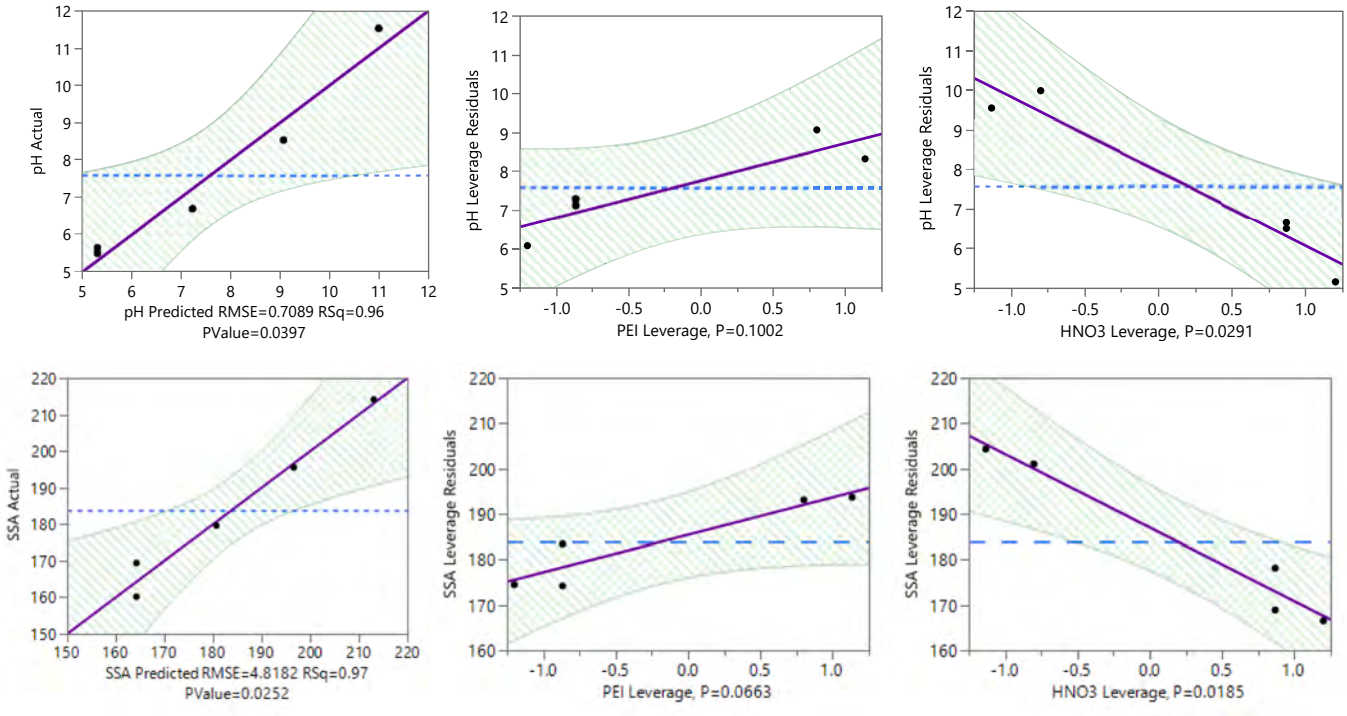

Fig. 2. Design of Experiments (DOE) for CZA-PEI pastes for: pH response factor (top row) and Specific Surface Area (SSA) response factor.

between particles of the same charge can be minimized. This leads to substantial reduction in viscosity and limits sedimentation, agglomeration and prevents nozzle-clogging. In addition, the sign of the charge might indicate compatibility issues, as opposite charges attract each other. Particles with positive charges, in this case the pure CZA in the pH range < 9.5 (see Fig. 1) will be attracted to particles with net negative charges, in this case the H-ZSM-5 zeolite. This results in agglomeration of particles and potential issues with stability, should they be added together in the same medium in this pH-region. This instability may result in instable paste rheology and lower solids content (due to an

Table 1
Selected design of experiments for screening of parameter influence on catalyst properties and catalytic performance; Inorganic Binder (IB), Solids Content (SC), and Methyl Cellulose (MC) binder content were varied.

Run	PEI	HNO_3	IB	MC
1	+1	−1	+1	−1
2	−1	+1	+1	+1
3	−1	+1	−1	−1
4	+1	+1	−1	+1
5	−1	−1	−1	+1

Table 2
Selected experimental values corresponding to the levels selected in the Design of Experiments (DOE). Values are calculated in wt.% with respect to the solids in the printing paste without the addition of the inorganic binder.

Level	PEI	HNO_3	IB	MC
−1	5 %	3.3 %	10 %	13 %
+1	15 %	15.4 %	19 %	23 %

Table 3
Resulting output variables investigated in the experiments and their values.

Run	pH	Load cell/N	SSA (BET)/m^2g^{-1}
1	11.52	89	214
2	5.65	306	160
3	5.50	820	169
4	6.69	358	180
5	8.54	313	196

increase in viscosity) that may in turn cause increased shrinkage and cracking during drying.

By adapting the surface charge of one of both components, the presence of opposite charged particles in the printing paste can be avoided, as well as the resulting instabilities. The authors tried to add a branched PEI (polyethyleneimine) based system. As this material is cationic in nature, it preferably attaches itself to the surface of the negatively charged H-ZSM-5 zeolite. The addition of the PEI to the zeolite directly makes the zeolite net positively charged (dark blue points in Fig. 1) while the total pH of the printing paste becomes higher when adding more PEI-solution. The addition of the PEI solution was also executed on the pure CZA-based particles. As evidenced in the light blue curve in Fig. 1, no unexpected changes to the surface charge of CZA happened by adding the PEI solution. Finally, a 'stabilized' suspension of H-ZSM-5 with PEI was created, and the effect of a pH reduction was investigated, to confirm if the combined material remained positively charged at that point. To summarize, the PEI addition to the H-ZSM-5

Table 4
Selected design of experiments for screening of parameter influence on mechanical properties and bending.

Run	PEI/HNO_3	IB	SC	MC	Drying
1	−1	−1	−1	−1	L2
2	−1	−1	+1	+1	L1
3	+1	−1	+1	−1	L3
4	+1	+1	+1	+1	L2
5	−1	+1	−1	+1	L3
6	+1	+1	−1	−1	L1
7	+1	−1	−1	+1	L1

Table 5
Selected experimental values corresponding to the levels selected in the second Design of Experiments. Values are calculated in wt.% with respect to the solids in the printing paste without the addition of the inorganic binder.

Level	PEI/HNO_3	IB	SC	MC	Drying
−1/ L1	13.3 %/3.7 %	8 %	60 %	13 %	Open drying @ 60 %RH
+1/ L2	20 %/5.5 %	12 %	62 %	20 %	Enclosed drying
L3					Climate chamber 80 %RH 20 °C

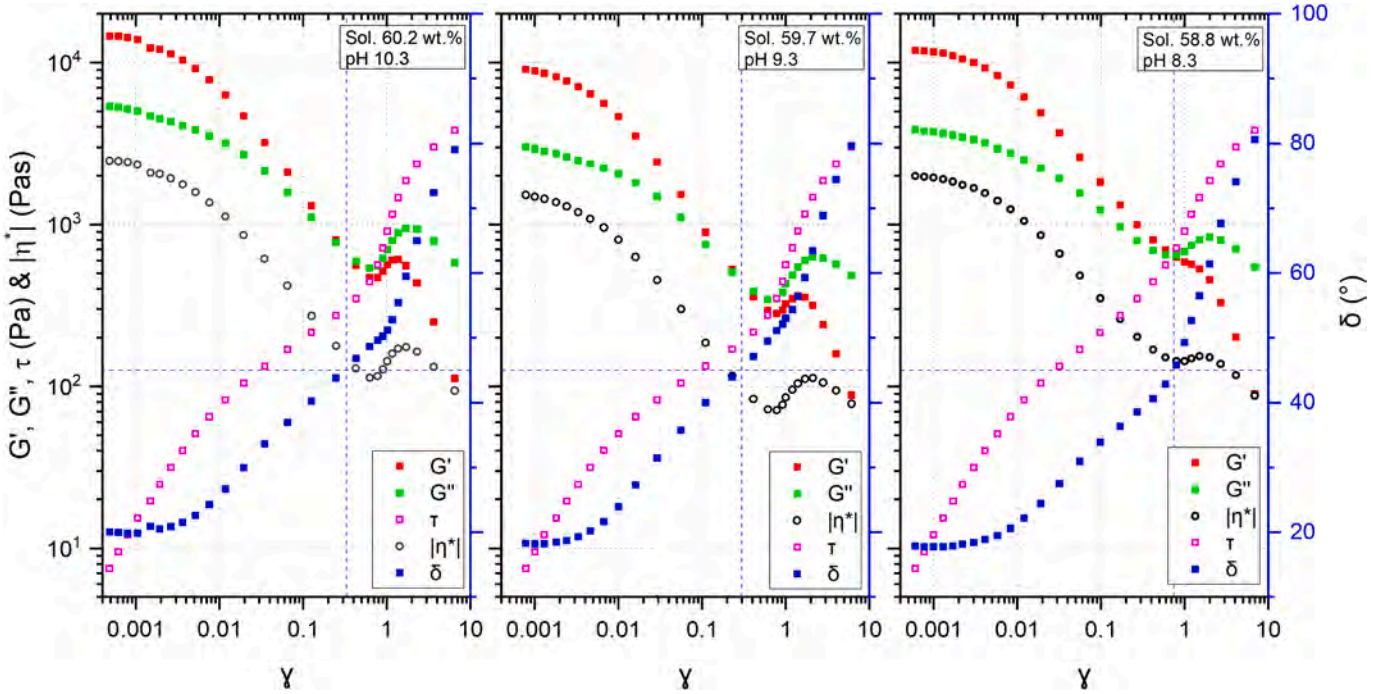

Fig. 3. Dynamic oscillatory rheological measurements (amplitude sweep results) on 3D-printing CZA:H-ZSM-5 pastes. Plots of the elastic (storage) modulus (G′), plastic (loss) modulus (G″), viscosity (|η*|), shear stress (τ) and phase angle (δ) as a function of sheer deformation (γ) correspond to (from left to right): pH values of 10.3, 9.3 and 8.3, and respective paste solids content of 60.15 wt%, 59.7 wt% and 58.8 wt%.

Table 6
Resulting output variables investigated in the utilized designed experiment and their values.

Run	pH	Load cell/ N	Cracks/fibers/ %	Curvature/ mm	$G' = G''$/ Pa	τ (@$G' = G''$)/ Pa	Yield point/ Pa	G' LVR/ Pa	Intraparticle porosity/ %	Crushing strength/ N
1	9.42	47.2	89	22	284	116	14	7,070	49.8	6.4
2	9.27	163.5	33	6.2	767	486	42	41,500	48.7	8.4
3	9.72	190.4	22	7.3	1,678	1,715	131	251,000	47.6	16.8
4	9.62	271.9	17	1.6	1,613	1,650	116	157,000	46.7	9.3
5	9.12	93.2	100	5.1	695	335	34	24,900	47.3	7.7
6	9.62	106.3	50	13	1,081	936	73	55,800	47.5	11.6
7	9.76	112.8	43	3.5	1,122	956	71	65,900	44.9	11.0

Fig. 4. Failure in printing CZA:H-ZSM-5 catalysts at an early stage.

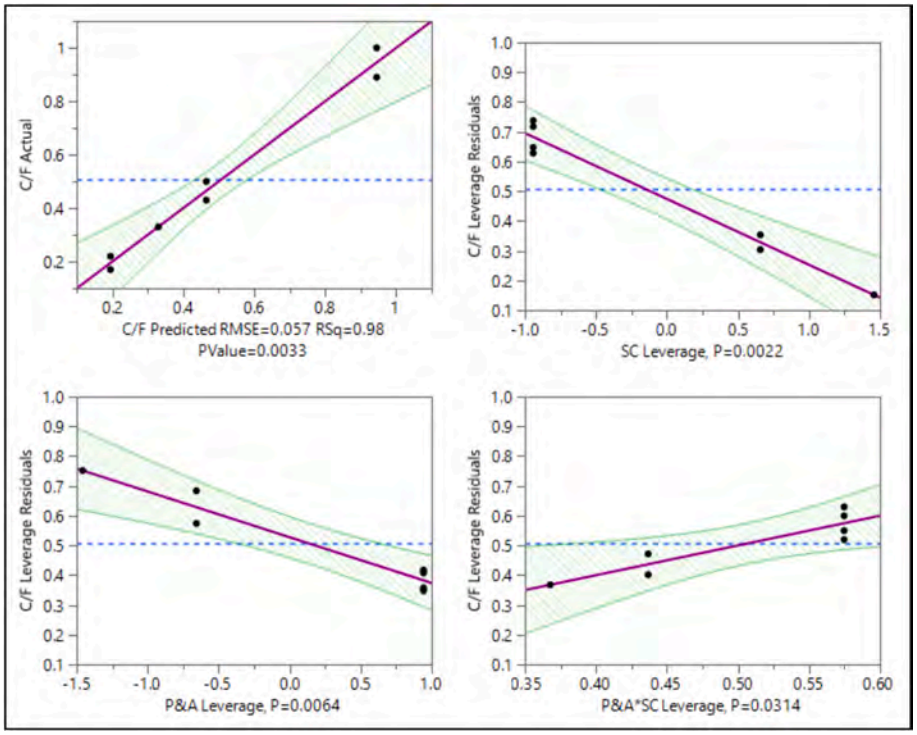

Fig. 5. Actual by predicted plot and related leverage plots for the amounts of cracks in the printed fibers (C/F) from the second Design of Experiments as function of (top left) cracks per fibers (C/F) using Root Mean Square Error (RMSE) as the standard deviation and the high correlation coefficient R-squared (RSq) and as function of important parameters including: (top right) solids content (SC, p = 0.0022), (bottom left) PEI and acid (P&A, p = 0.0064) and (bottom right) the interaction between these two (P&A*SC, p = 0.0314).

resulted in both components having the same net (positive) charge in the pH range during printing. This resulted in internal compatibility and preventing issues related to nozzle clogging and instability.

After ensuring compatibility between the components in the paste, a Design of Experiment was utilised to investigate the interrelation between the paste composition and the effect of the paste composition on the properties of the printed catalyst, which have an influence on the activity. The properties included Specific Surface Area (SSA) of the final calcined catalyst, as well as the pH of the printing paste.

3.2. DOE – catalytic activity

In the initial Design of Experiments, the investigated output variables were pH, load cell (indicating the printability of the printing ink) and the specific surface area of the catalyst material calcined at 425 °C after printing. While the broad range utilized for all input parameters did not give a printable paste for all runs, the large variation in output parameter results made it possible to link input and output parameters, enabling further finetuning during further experimentation.

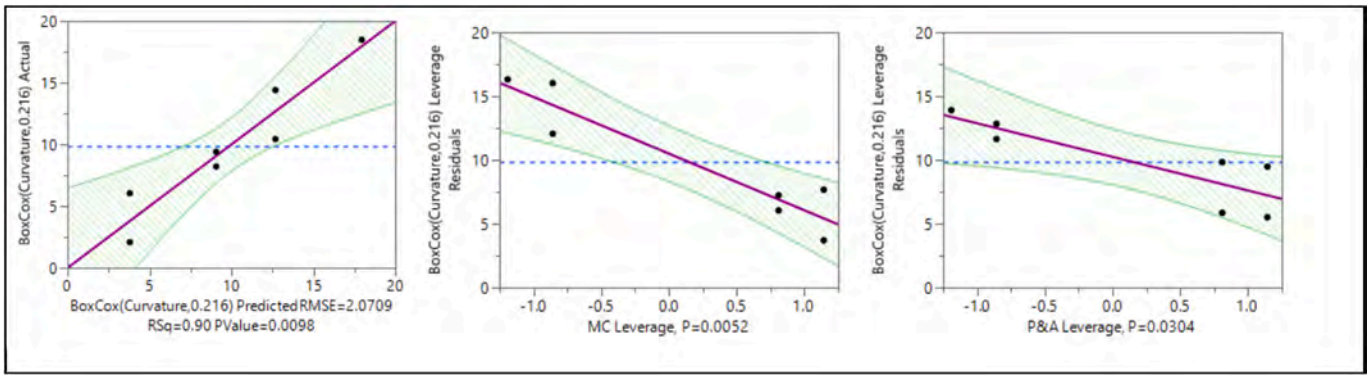

Fig. 6. Actual by predicted plot and related leverage plots for the amounts of curvature in the printed fibers from the second design of experiments.

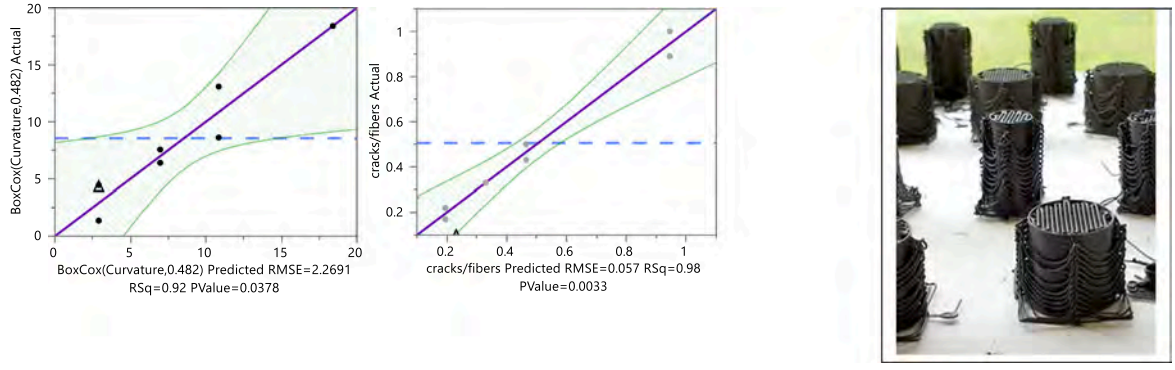

Fig. 7. Left and middle: plots avoiding cracks and bending – verification run (triangle). Right: resulting 3D printed structures, based on scale-up of optimised procedure.

The screening experiments from the first DOE successfully highlighted the link between the paste composition and resulting pH and specific surface area. For each output parameter, a model was built with respective correlation coefficients of 0.97 and 0.96. The fitting of both calculated values through the model and the experimental data are included in Fig. 2. Interestingly, both amounts of HNO_3 and PEI significantly altered the pH of the printing paste as well as the specific surface area of the final calcined catalyst. It is logical that larger amounts of PEI increase the pH due to the increase in the amount of amine functional groups present in the paste. It is also logical that HNO_3, as an acid, decreases the pH. Although the model's results are readily explained, the correlation is still interesting as it can be used to work towards the desired pH value during subsequent experiments, when combining both acid and PEI.

However, the influence of the paste composition on the specific surface area of the printed calcined catalyst is of more interest. Its value is slightly unexpected: both acid and PEI affected the specific surface area, and their influence is more significant than the addition of 9 % more inorganic binder (which effect in the utilized range and with the limited set of experimental runs is not deemed statistically significant). The same trends can be observed for the influence of both components on the pH and specific surface area. Therefore, the correlation between both output parameters is of interest too, as shown in Fig. 2. This figure shows a strong correlation between the pH value of the fresh paste and the final specific surface of the calcined catalyst. This is of great importance, as it can affect catalytic results of 3D printed catalysts. During the assessment of the early results in the project, poor catalytic performance (versus the original powder catalyst) was attributed to a drop in specific surface area. Therefore, it was essential to address the reason behind this drop. After assessing these parameters, it was found that the pH of the printing paste is crucial to the resulting print. A reduction in specific surface area at lower pH values can be explained by H-ZSM-5 zeolite degradation (dealumination) and possible CZA dissolution. For the printing of future CZA:H-ZSM-5 catalysts, a paste pH below 9 should be avoided, according to the models.

Table 1 includes the selected design of the experiment to screen the influence of a changing composition of the printing paste on the properties of the printed catalysts. By convention, −1 and +1 indicate the edges of the parameter space investigated in the series of experiments. For the various parameters, the values were defined by comparison to the mass of solids in the printing paste. These values are included in Table 2. For PEI, −1 and +1 respectively indicate the addition of PEI in an amount corresponding to 5 wt% and 15 wt% of the total solids in the paste. While the amount of PEI was calculated with respect to the total amount of solids in the paste, the amounts of HNO_3, inorganic binder and MC-binder were calculated with respect to the weight of catalyst (without inorganic binder) in the paste. Specific values can be found in Table 2. Water was adjusted appropriately to ensure a solids content in the paste of approximately 58.5 wt%. Table 3 gives an overview of the resulting output variables investigated in the experiments and their values.

It should be noted that pastes generated within run 2, 3 and 4 resulted in agglomerates blocking the nozzle from time to time during printing. Paste 1 was too liquid for printing, which was clear from the very low load on the syringe during printing (load cell value). In addition, the paste from this experiment exhibited phase separation. Although the pastes themselves were not resulting in good structures, they could be dried and calcined and subjected to measurement of the Specific Surface Area (SSA), determined using Brunauer-Emmett-Teller (BET) analysis (shown in Table 3).

3.3. DOE – mechanical integrity and printability

The next strategy focussed on improving the mechanical integrity of

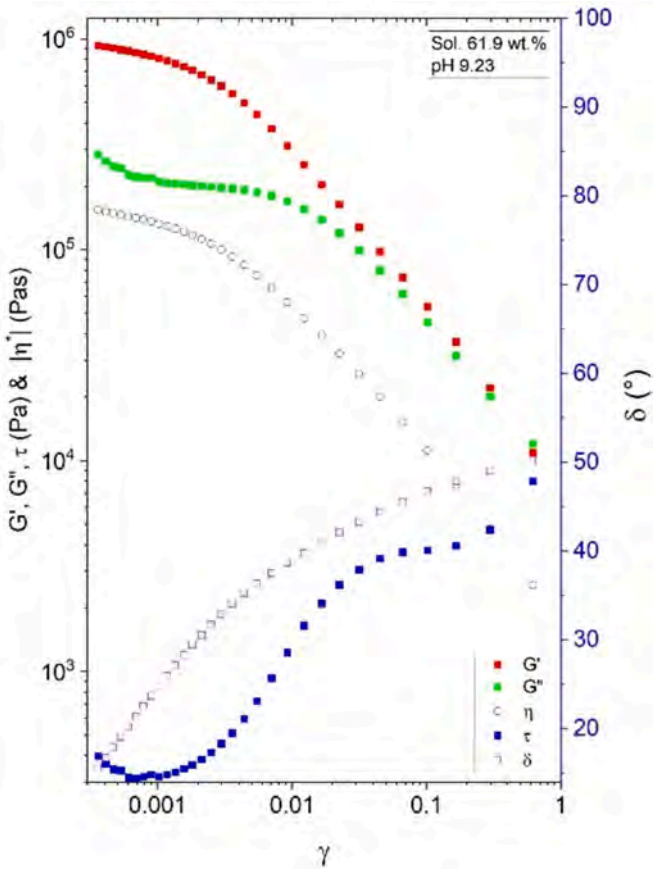

Fig. 8. Rheology data from oscillation sweep measurements on final scaled up CZA:H-ZSM-5 (PEI-based) 3D-printing paste.

the printed catalysts. After printing, several factors may affect the structural integrity of printed catalysts. These factors include warping and bending during drying, cracking. In addition, the mechanical integrity is influenced by the amount and type of inorganic binder in the printing paste.

To improve the mechanical integrity of printed CZA:H-ZSM-5 catalysts, a second Design of Experiments was executed. However, to be able to draw meaningful conclusions from the DOE, pastes with decent printability had to be achieved. In the first series of experiments, it was shown that lower pH-values and a pH value at 11.5 led to issues with agglomerates and low viscosity/phase separation, respectively. Therefore, a closer assessment was made of the pH range where printable pastes could be made. With earlier observations regarding catalytic activity, three pastes with a pH value in the range of 8 – 10.5 were made (pH at second day, before printing of 8.3, 9.3 and 10.3). Afterwards, printability and rheology were investigated. Furthermore, the earlier relation of the ratio of HNO_3:PEI and the paste pH was confirmed.

Fig. 3 includes the data from the dynamic oscillatory rheological measurements as a standard means of characterising the viscoelastic properties of the pastes with different pH values and correlating the paste rheology with its printing performance. The curves show typical (shear-thinning) rheological behaviour for the CZA:H-ZSM-5 pastes suitable for 3D printing through micro-extrusion: a drop in viscosity with increasing stress. Also the viscoelastic properties linked to the printability and shape retention of the printing pastes can be assessed from these curves.

Several trends can be observed in the curves in Fig. 3. Although all pastes were printable, there were differences in pH and solids content yields between pastes, with slight differences in the stresses at the linear viscoelastic range (G' and G''), yield point, the crossover point (when $G' = G''$), and overall viscosity. At high pH, the crossover point occurred at a yield stress of 304 Pa. Decreasing the pH to 9.3 almost halved this yield stress to 185 Pa. Further lowering the pH to 8.3 doubled the original yield stress back to 645.6 Pa. The Yield point calculated based on G' at high pH amounted to 19 Pa. Decreasing the pH to 8.3 lowered the yield point to 18 Pa, while further lowering the pH to 8.3 increased the yield point to 24 Pa. The storage and loss moduli (G' and G'') and complex dynamic viscosity ($|\eta^*|$) showed similar trends. These observations, coupled with the measured solids content, indicates that lower pH values in the investigated range have an unwanted effect on the rheology of the printing pastes which results in a lower achievable solids content. Fig. 3 essentially shows that an optimal pH value of the paste, from a rheological point of view, is in the range of 9 – 10. This is confirmed by load cell data of respectively 170 N, 85 N and 140 N during the printing of these pastes.

After determining the right pH values through earlier SSA-measurements (the first Design of Experiments) and finetuning this range through rheological experiments, a second Design of Experiments was executed, during which the ratio between HNO_3 and PEI was fixed, to reach approximate appropriate pH values. The total amounts of PEI/HNO_3, inorganic binder (IB) content, solids content (SC), and methyl cellulose (MC) binder content were varied (see Table 4). The drying procedure was also varied.

Fig. 9. Scaling up of CZA-based 3D printed catalysts.

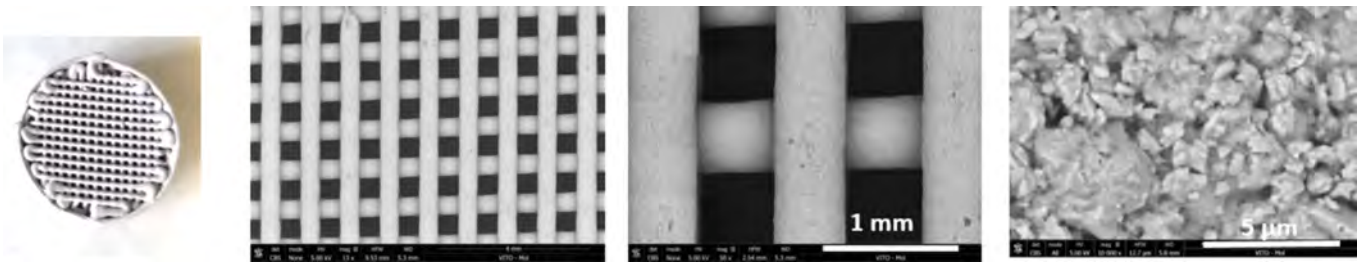

Fig. 10. Photo and SEM images of representative H-ZSM-5 cylinders (ø14 mm diameter) containing typically 80.4 wt% H-ZSM-5, 7.3 wt% bentonite and 12.3 wt% silica binder.

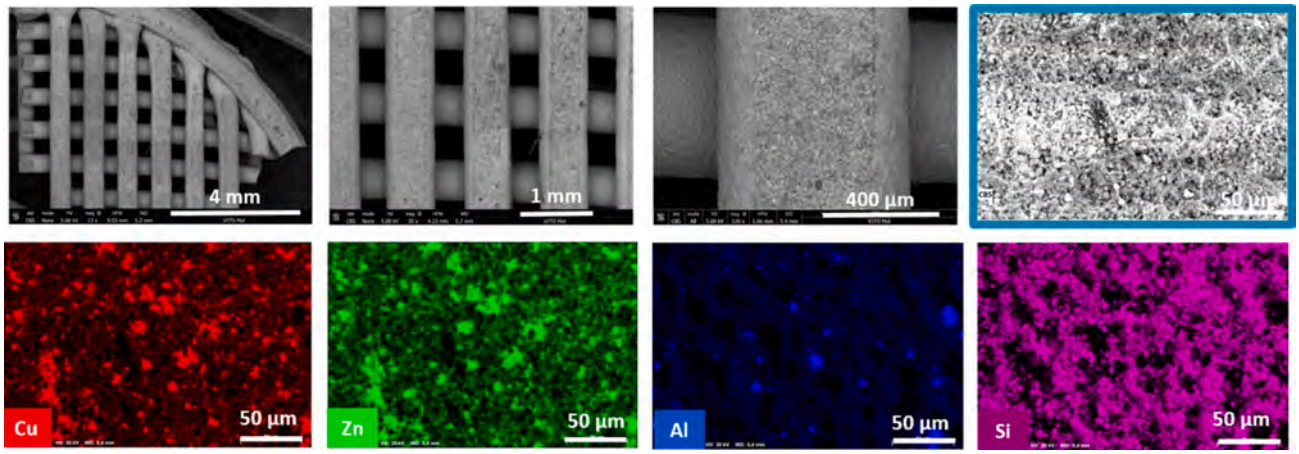

Fig. 11. SEM/EDS images (top view) of optimized 3D printed 21,047 CZA:H-ZSM-5 (PEI-based) monoliths (ø14 mm diameter) composed of 50:50 ratio of CZA:H-ZSM-5 (42.65 wt% CZA + 42.65 wt% H-ZSM-5 + 14.7 wt% AL2O3 BINDER).

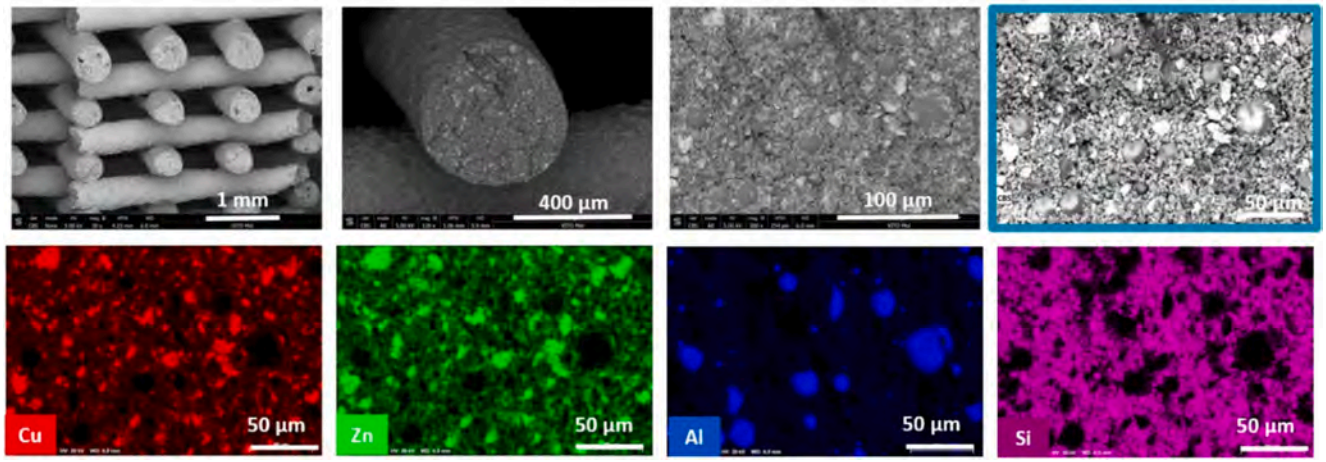

Fig. 12. SEM/EDS images (vertical cross-section) of optimized 3D printed 21,047 CZA:H-ZSM-5 (PEI-based) monoliths (ø14 mm diameter composed of 50:50 ratio of CZA:H-ZSM-5 (42.65 wt% CZA + 42.65 wt% H-ZSM-5 + 14.7 wt% AL2O3 BINDER)).

The input variables were adjusted to similar values as the ones used within the first Design of Experiments, mainly in order to achieve printable materials. As the earlier experiments had shown, printable pastes could be achieved with a paste composition with a pH value between 9 and 10 while keeping the solids content between 60 % and 62 % (see Table 5). This pH range also ensured sufficient catalytic activity for CZA-based catalysts.

The resulting output variables are included in Table 6. The investigated parameters included pH, load cell during printing, elastic and loss moduli at the crossover point, the yield stress at the crossover point, the yield point, the storage modulus in the LVR region, the intraparticle porosity of calcined printed materials and the final crushing strength of printed fibers. Two parameters included in Table 6 need further explanation, i.e. (i) cracks/fibers and (ii) curvature.

As initial screening has shown, the mechanical strength of 3D printed materials is a complex concept. Initially, the aim was to avoid printed structures which failed to hold their printed structure, due to (i) cracks originating from bending or (ii) failure during drying or (iii) generally poor mechanical strength leading to breakage during handling. Some of these structures are included in Fig. 4 (left).

In order to obtain a clear measure of the parameters leading to cracks and bending, the authors analysed parameters that offered quantifiable

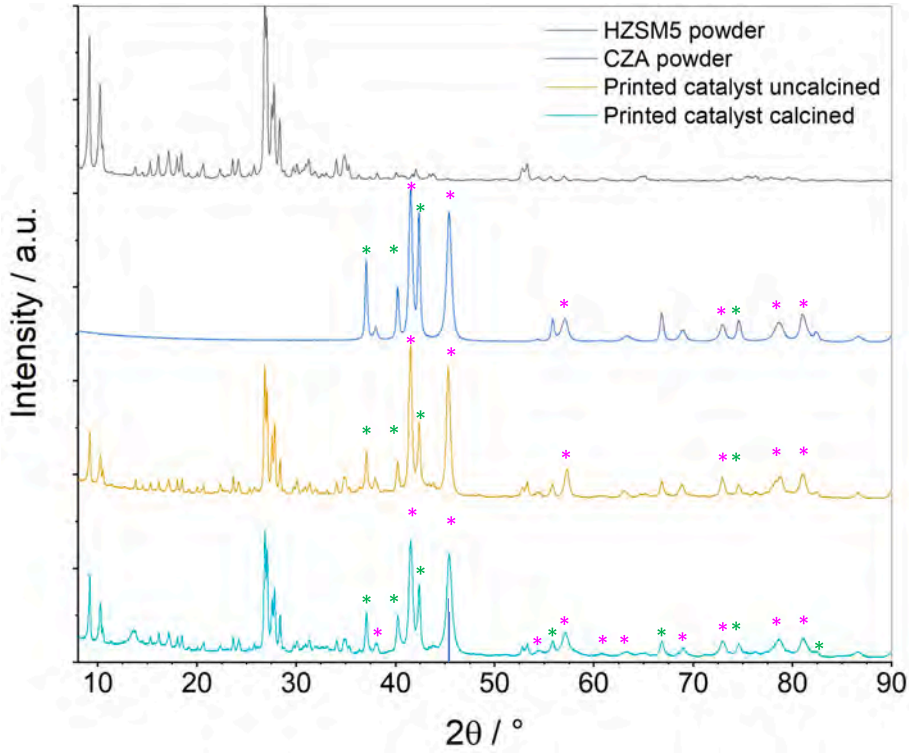

Fig. 13. XRD patterns of calcined H-ZSM-5 and CZA catalyst starting powders and 3D printed CZA:H-ZSM-5 catalyst before and after calcination showing the main peaks that can be assigned to Zn and Cu oxide phases (*CuO, *ZnO).

results that could be utilized in the design of experiments. The most straightforward manner of comparing different pastes was to print different straight fibers in a fixed pattern with the same printing conditions, on the same printing substrate, and evaluate bending and cracking of these printed fibers. Curvature is the total height reached by the bending of the fibers in mm. 20 mm means that the end of the fiber was bent into the air, reaching 20 mm of height perpendicular to the table after drying. 1.6 mm means that the fiber did not bend significantly, as this value approaches the thickness of all printed fiber during the experiments. Therefore, higher values indicate more bending of the printed fibers after drying. On the other hand, the results provided under 'cracks/fibers' show the value calculated when counting the number of visible cracks of the (fully printed) fibers, divided by the total number of fibers investigated in the experiment. 22 %, for example, means 2 cracks in a set of 9 fully printed fibers. The very large variation of results can be seen in Fig. 4 (right) indicating a large influence of the utilized parameters on the printed structures.

Not all investigated output parameters showed meaningful trends, due to the complexity of the processes. However, both curvature and cracks/fibers showed a meaningful indication of which paste composition could lead to 3D-printed structures with improved mechanical properties. From the rheology side, Yield point and storage modulus (G') of the printing pastes could be well correlated with the paste composition.

Fig. 5 shows the actual by predicted plot for the cracks per fibers (C/F) with important parameters including solids content (SC, $p = 0.0022$), PEI and acid (P&A, $p = 0.0064$) and the interaction between these two (P&A * SC, $p = 0.0314$), all included in the model. The high correlation coefficient ($R^2 = 0.98$) indicates an excellent correlation between the parameters included in the model and the output variable. Fig. 5 also contains the leverage plots of the variables included in the model. These leverage plots give an indication of the variability explained by the specific parameter when it is included in the model. Especially an increase in solids content (SC, $p = 0.0022$) and an increase in PEI, while keeping enough acid to achieve an appropriate pH (PEI/HNO_3, $p = 0.0064$) result in a significant decrease in cracks in the printed CZA:H-ZSM-5 catalysts within the Design of Experiments. The interaction parameter means that at a higher value of either PEI and acid, or of the solids content, there is less effect of the other parameter (improving the robustness of the recipe). Other parameters did not have a statistically significant effect.

Fig. 6 shows the actual by predicted plot for the curvature with important parameters including the percentage of methyl cellulose (MC, $p = 0.0052$) and the percentage of PEI and HNO_3 (PEI&HNO3, $p = 0.0304$), i.e. both organic binders. The correlation coefficient of 0.90 indicates a decent correlation between the observed values and the values calculated in the model. The output parameter (Curvature) was transformed through a box-cox transformation ($\lambda = 0.216$) to ensure normality of the data. The leverage plots show that an increase in percentage of both methyl cellulose and of PEI ensures lower curvature and thus less bending of the fibers after printing. Other parameters did not have a statistically significant effect.

In summary, after optimization, high PEI content and high solids content led to a reduction in the number of cracks in the final structures ($R^2 = 0.98$). The bending of fibres and structures was avoided by utilizing enough organic binder and a high PEI content ($R^2 = 0.92$). All input variables were simultaneously optimized in a final recipe. The effect of this final composition was verified with a verification run (see triangle in Fig. 7). The results show the suitability of this optimized composition for upscaling the paste production, while keeping excellent mechanical integrity. Fig. 7 also includes a picture of printed structures after the scale-up of the optimized procedure.

See Supplementary Figure S1 for resulting intercorrelation between pH and specific surface area. For more details on the full printing paste optimization (second Design of Experiments) see the Supplementary Material where Figures S2-S5 and Table S1 show respectively: predicted plot and related leverage plots for the yield point; yield stress; the pH of the printed pastes; as well as a relative magnitude of effects in the model versus strongest effect for each variable.

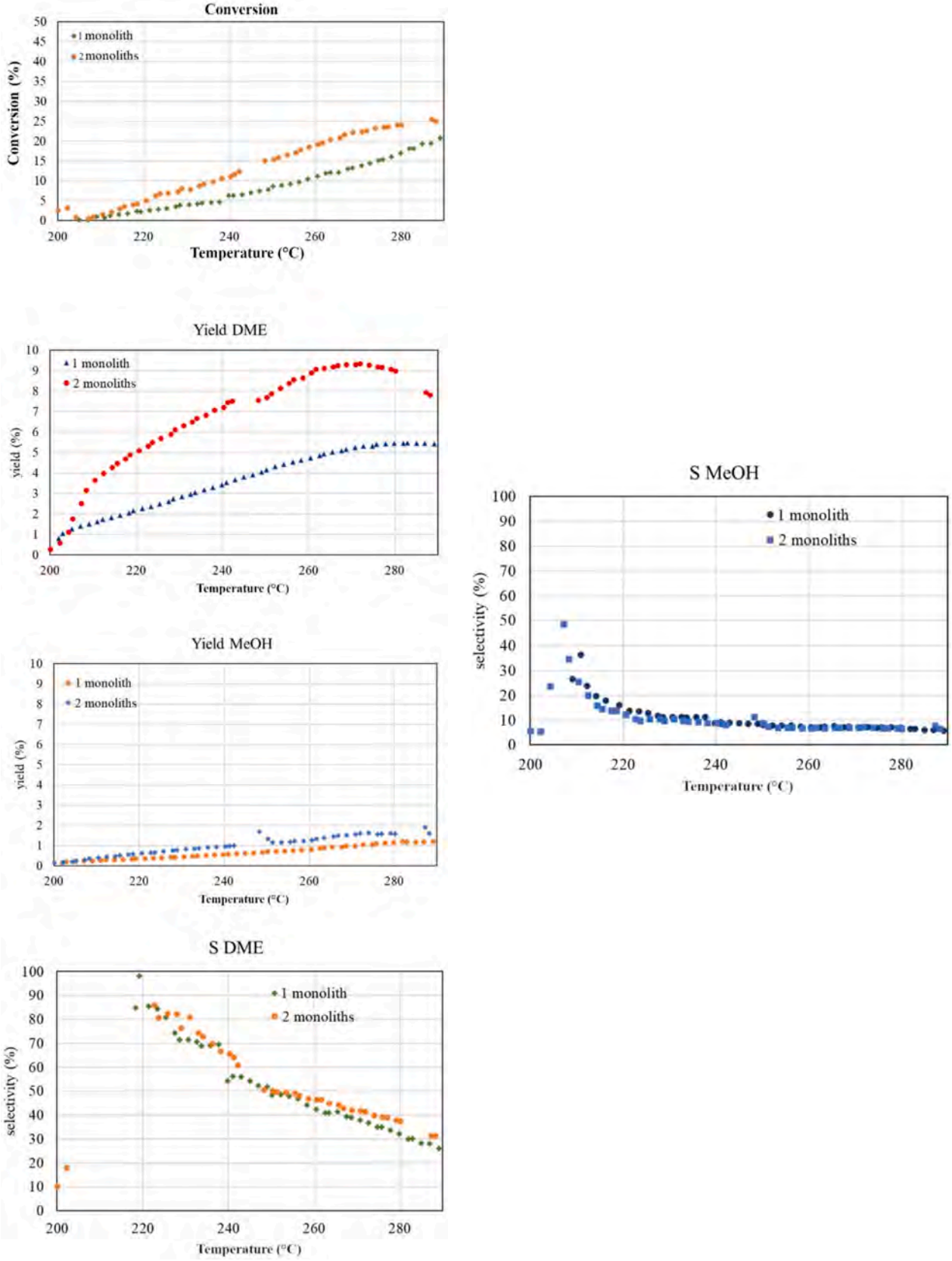

Fig. 14. Conversion, DME and methanol yield and DME and methanol selectivity for the initial temperature sweep experiments on the printed monolith reactors.

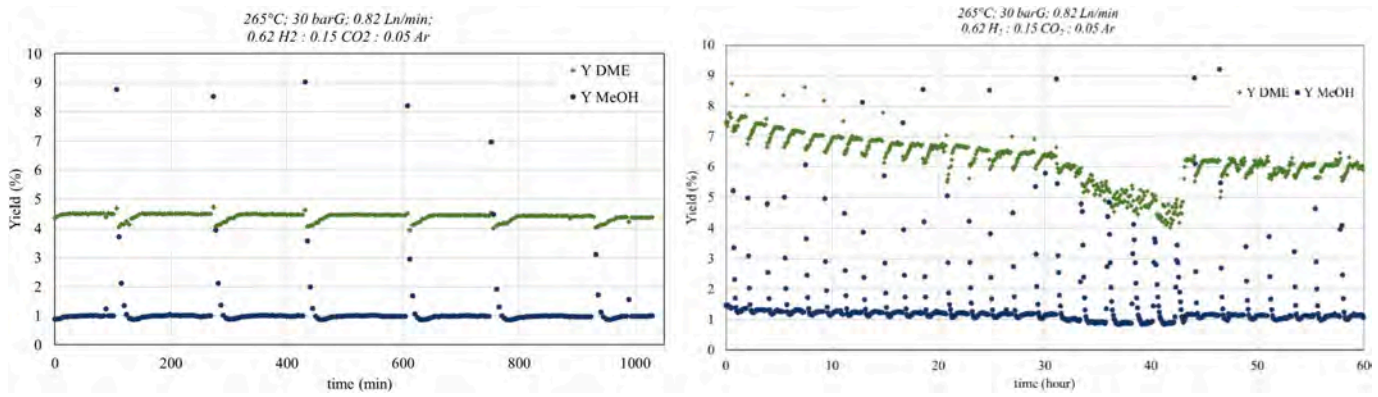

Fig. 15. Duration experiments of printed single monolith reactor (left) and printed stacked double monolith reactor (right) indicating yield of both dimethyl ether and methanol.

3.4. 3D printed catalyst for DME production – scaling up

After optimizing the printing of catalyst monoliths with 1:1 wt of catalyst and co-catalyst at small scale, the work focused on preparing the catalyst ink at a higher amount, suitable for printing multiple structures. The scaled-up printing pastes had a pH of 9.23 and consisted of 42.65 wt % CZA, 42.65 wt% H-ZSM-5 and 14.7 wt% of inorganic binder. The yield point, storage modulus and crossover point were respectively 1.04 10^3 Pa, 9.3 10^5 Pa, 1.66 10^4 Pa, as can be seen in the oscillatory sweep rheology measurement included in Fig. 8 (for more details see Supplementary Figure S6). Fig. 9 shows the final scaled up 3D printing. Subsequently, the printer was equipped with up to 6 syringes, printing up to 42 catalyst structures of ø14 mm diameter per batch (see Fig. 9).

3.5. Characterisation of printed catalysts

Figs. 10, 11 and 12 include SEM/EDS images from respectively pure printed H-ZSM-5, and the optimized CZA:H-ZSM-5 catalyst (both top view and vertical cross section). The top view shows the excellent stability of the printing paste, resulting in structures that keep their structural integrity after printing. The SEM/EDS images display the excellent homogeneity of the catalyst as all CZA components and Si (from the zeolite) are all well dispersed in the structure.

Fig. 13 shows the XRD patterns of the printed structure after calcination, together with the XRD patterns of the constituent powdered catalyst and co-catalyst. Characteristic peaks from both zeolite and mixed oxides are identified.

3.6. Catalytic measurements

The printed monolithic catalyst was tested for its performance for CO_2 reduction to DME (see Figs. 14 and 15). A standard temperature sweep showed a profile similar to the values reported in our previous paper (Bonura et al., 2023), with the powdered catalyst test. However, the conversion and yield of the reaction test on the single monolith appear a bit lower. This is most likely the result of a much higher Weight hourly space velocity (WHSV) (~11 NL/gcat/h versus 1 NL/gcat/h). The test on the double monolith reactor with the same gas flow rates shows the increased conversion and yield as a result of the lower WHSV (~5.2 LN/gcat/h), but the selectivity is similar. It appears that the selectivity for DME decreases with temperature (60–30 % between 240–290 °C), while the selectivity towards methanol stays at a similar level (10–8 % between 240–290 °C).

After the temperature sweeps for each respective catalyst, the reactor was set to 265 °C. The reaction was run at this temperature for >1000 min (17 h) for the single monolith reactor and 60 h for the stacked monolith reactor. The yield showed some spikes which are the result of condensation of products in the exhaust lines (quite some water is produced during the reaction), but the general trend is very promising. Overall, the deactivation in this run looks almost linear, decreasing the DME yield with ~0.18 % per 24 h.

As the conversion on the stacked monolith reactor is much higher, there are increased issues related to the condensation of water in the exhaust line, but the trend is clear. Initially, there is some deactivation, with the yield dropping from 7.8 % to 6.2 % DME, but after approximately 40 h, the DME yield remains stable at around 6.1 %.

4. Conclusions and further work

This work has shed light on the optimization procedures for printing formulations for dual phase CZA:H-ZSM-5 catalyst systems. A series of monoliths of the CZA:H-ZSM-5 catalyst formulation were printed with defined shapes and desired properties, including the level of solid and binder content, pH, resulting specific surface area and catalytic activity.

We were able to demonstrate stable formulations during and after the printing process by selecting critical criteria for the suitability for upscaling of the printing paste production, while retaining excellent mechanical integrity of the resulting material post printing. To achieve the desired improvement of the 3D printing process, the methodology relied on Design of Experiments (DoE), which revealed the physical processes while minimising the number of preparation experiments. It was shown that DoE provided a clear understanding of the parameters causing cracks and bending of the 3D printed structures. The parameters offered quantifiable results (leverage plots) at up to 99 % confidence level (expressed as correlation coefficients R^2 of up to 0.99), that could be applied in the optimization step. The optimisation demonstrated the effect of the composition and rheological properties of the printing paste on the structural stability and performance of the resulting printed catalysts. After successful paste optimization, the final 3D-printed catalysts were scaled up and evaluated in a single-tube catalytic reactor. The catalytic tests showed similar conversions and selectivities to previously reported measurements on powder catalysts, demonstrating the success of this printing paste optimization and printing of the catalyst structures.

CRediT authorship contribution statement

Yoran De Vos: Writing – original draft, Visualization, Validation, Methodology, Formal analysis, Data curation, Conceptualization. **Arie J.J. Koekkoek:** Visualization, Methodology, Formal analysis, Data curation. **Giuseppe Bonura:** Methodology, Data curation, Conceptualization. **Serena Todaro:** Formal analysis, Data curation. **Monika Kus:** Methodology. **Alexander Vansant:** Methodology, Investigation. **Gijsbert Gerritsen:** Methodology, Data curation, Conceptualization. **Catia Cannilla:** Supervision, Methodology. **Hendrikus C.L. Abbenhuis:** Investigation, Funding acquisition, Conceptualization. **Vesna**

Middelkoop: Writing – review & editing, Writing – original draft, Methodology, Investigation, Funding acquisition, Data curation, Conceptualization.

Declaration of competing interest

The authors declare that they have no known competing financial interests or personal relationships that could have appeared to influence the work reported in this paper.

Acknowledgements

We would like to thank Myrjam Mertens and Raymond Kemps for their assistance with XRD and electron microscopy respectively.

Funding Information: this work was part of the CO2Fokus project, which received funding from the European Union's Horizon 2020 research and innovation programme under the Grant Agreement No.838061.

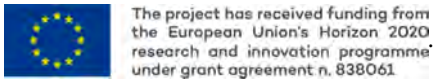

This document reflects only the authors' view and the Climate Innovation and Networks Executive Agency (CINEA) and the European Commission are not responsible for any use that may be made of the information it contains.

Appendix A. Supplementary material

Supplementary data to this article can be found online at https://doi.org/10.1016/j.mseb.2024.117759.

Data availability

Data will be made available on request.

References

[1] G.A. Olah, Towards oil independence through renewable methanol chemistry, Angew. Chem. Int. Ed. 52 (2013) 104–107.
[2] G.A. Olah, A. Goeppert, G.K.S. Prakash, Beyond Oil and Gas: The Methanol Economy, 2nd ed., Wiley-VCH, Weinheim, 2009.
[3] S. Perathoner, G. Centi, CO2 recycling: a key strategy to introduce green energy in the chemical production chain, ChemSusChem 7 (2014) 1274–1282.
[4] C. Liu, Z. Liu, Perspective on CO2 hydrogenation for dimethyl ether economy, Catalysts 12 (11) (2022) 1375, https://doi.org/10.3390/catal12111375.
[5] Noelia Mota, Elena Millán Ordoñez, Bárbara Pawelec, José Luis G. Fierro, Rufino M. Navarro, Direct synthesis of Dimethyl Ether from CO2: recent advances in bifunctional/hybrid catalytic systems, Catalysts 11(4) (2021) 411. doi: 10.3390/catal11040411.
[6] Giuseppe Bonura, Serena Todaro, Catia Cannilla, Francesco Frusteri, CO2 hydrogenation into dimethyl ether Conventional and innovative catalytic routes in The Carbon Chain in Carbon Dioxide Industrial Utilization Technologies, 2022, CRC Press.
[7] S. Afandizadeh, E.A. Foumeny, Design of packed bed reactors: Guides to catalyst shape, size and loading selection, Appl. Therm. Eng. 21 (2001) 669–682, https://doi.org/10.1016/S1359-4311(00)00072.
[8] K.G. Allen, T.W. von Backström, D.G. Kröger, Packed bed pressure drop dependence on particle shape, size distribution, packing arrangement and roughness, Powder Technol. 246 (2013) 590–600, https://doi.org/10.1016/j.powtec.2013.06.022.
[9] M. Frey, D. Édouard, A.-C. Roger, Optimization of structured cellular foam-based catalysts for low-temperature carbon dioxide methanation in a platelet milli-reactor, Comptes Rendus Chim. 18 (2015) 283–292.
[10] D. Schollenberger, S. Bajohr, M. Gruber, R. Reimert, T. Kolb, Scale-up of innovative honeycomb reactors for power-to-gas applications – The Project Store & Go, Chemie Ing. Tech. 90 (2018) 696–702, https://doi.org/10.1002/cite.201700139.
[11] S. Danaci, L. Protasova, V. Middelkoop, N. Ray, M. Jouve, A. Bengaouer, P. Marty, Scaling up of 3D printed and Ni/Al2O3 coated reactors for CO2 methanation, React. Chem. Eng. 4 (2019) 1318.
[12] Andrea Montebelli, Carlo Giorgio Visconti, Gianpiero Groppi, Enrico Tronconi, Stefanie Kohler, Hilde Johnsen Venvik, Rune Myrstad, Washcoating and chemical testing of a commercial Cu/ZnO/Al2O3 catalyst for the methanol synthesis over copper open-cell foams, Appl. Catal. A 481 (2014) 96–103.
[13] I. Pérez-Miqueo, O. Sanz, M. Montes, Structuring Cu/ZnO/Al2O3 catalyst for methanol synthesis: slurry additive effect in the washcoating method, Chem. Eng. Process. - Process Intesif. 182 (2022) 109210.
[14] V. Middelkoop, T. Slater, M. Florea, F. Neatu, S. Danaci, V. Onyenkeadi, K. Boonen, B. Saha, I.A. Baragau, S. Kellici, Next frontiers in cleaner synthesis: 3D printed graphene-supported CeZrLa mixed-oxide nanocatalyst for CO2 utilisation and direct propylene carbonate production, J. Clean. Prod. 214 (2019) 606–614.
[15] T. Karsten, V. Middelkoop, D. Matras, A. Vamvakeros, S. Poulston, V. Grosjean, B. Rollins, F. Gallucci, H.R. Godini, S.D.M. Jacques, A.M. Beale, J.-U. Repke, Multi-scale studies of 3D Printed Mn–Na–W/SiO2 catalyst for oxidative coupling of methane, Catalysts 11 (3) (2021) 290.
[16] C. Jacquot, V. Middelkoop, A. Koeckritz, A. Pohar, R. Bienert, S. Kellici, I.-A. Baragau, B. Venezia, A. Gavriilidis, B. Likozar, A.M. Beale, 3D printed catalytic reactors for aerobic selective oxidation of benzyl alcohol into benzaldehyde in continuous multiphase flow, Sustain. Mater. Technol. 30 (2021).
[17] C.R. Tubío, J. Azuaje, L. Escalante, A. Coelho, F. Guitián, E. Sotelo, A. Gil, 3D printing of a heterogeneous copper-based catalyst. J. Catal. 334 (2016) 110–115.
[18] V. Middelkoop, A. Vamvakeros, D. De Wit, S. Jacques, S. Danaci, C. Jacquot, Y. De Vos, D. Matras, S. Price, A. Beale, 3D printed Ni/Al2O3 based catalysts for CO_2 methanation: a comparative and operando XRDCT study, J. CO2 Util. 33 (2019) 478–487, https://doi.org/10.1016/j.jcou.2019.07.013.
[19] Clement Jacquot, Antonis Vamvakeros, Andraž Pavlišič, Stephen W.T. Price, Hongyang Dong, Dorota Matras, Lidia Protasova, Blaž Likozar, Simon D.M. Jacques, Andrew M. Beale, Vesna Middelkoop, A multi-scale study of 3D printed Co-Al2O3 catalyst monoliths versus spheres, Chem. Eng. J. Adv. 16 (2023) 100538.
[20] Leon R.S. Rosseau, Vesna Middelkoop, Hans A.M. Willemsen, Ivo Roghair, M. Van Sint Annaland, Review on Additive Manufacturing of Catalysts and Sorbents and the Potential for Process Intensification, Front. Chem. Eng., 2022, Materials Process Engineering, https://doi.org/10.3389/fceng.2022.834547.
[21] H. Bikas, P. Stavropoulos, G. Chryssolouris, Additive manufacturing methods and modelling approaches: a critical review, Int. J. Adv. Manuf. Technol. 83 (2016) 389–405, https://doi.org/10.1007/s00170-015-7576-2.
[22] S. Lawson, X. Li, H. Thakkar, A.A. Rownaghi, F. Rezaei, Recent advances in 3D printing of structured materials for adsorption and catalysis applications, Chem. Rev. 121 (2021) 6246–6291, https://doi.org/10.1021/acs.chemrev.1c00060.
[23] X. Zhou, C. Liu, Three-dimensional printing for catalytic applications: current status and perspectives, Adv. Funct. Mater. 27 (2017).
[24] C. Parra-Cabrera, C. Achille, S. Kuhn, R. Ameloot, 3D printing in chemical engineering and catalytic technology: structured catalysts, mixers and reactors, Chem. Soc. Rev. 47 (2018) 209–230.
[25] S. Wei, Xu. Guifang Han, J.S. Zhang, W. Wang, J. Zhang, Z. Zhang, W. Zhang, J. Zhang, L. Yang, J. Li, Y. Qiao, Preparation of excellent performance ZTA ceramics and complex shaped components using digital light processing 3D printing technology, J. Alloy. Compd. 980 (2024) 173640, https://doi.org/10.1016/j.jallcom.2024.173640.
[26] K. Wang, J. Yin, X. Chen, L.i. Wang, H. Xiao, X. Liu, Z. Huang, Advances on direct selective laser printing of ceramics: An overview, J. Alloy. Compd. 975 (2024) 17282, https://doi.org/10.1016/j.jallcom.2023.172821.
[27] R. Gadow, F. Kern, A. Killinger, Manufacturing technologies for nanocomposite ceramic structural materials and coatings, Mater. Sci. Eng. B 148 (1–3) (2008) 58–64, https://doi.org/10.1016/j.mseb.2007.09.066.
[28] M. Jabbari, R. Bulatova, A.I.Y. Tok, C.R.H. Bahl, E. Mitsoulis, J.h., Hattel Ceramic tape casting: A review of current methods and trends with emphasis on rheological behaviour and flow, Mater. Sci. Eng. B 39–6 (2016), https://doi.org/10.1016/j.mseb.2016.07.011.
[29] L. del-Mazo-Barbara, M.-P. Ginebra, Rheological characterisation of ceramic inks for 3D direct ink writing: A review, J. Eur. Ceram. Soc. 41 (2021) 18–33, https://doi.org/10.1016/j.jeurceramsoc.2021.08.031.
[30] G. Bonura, S. Todaro, V. Middelkoop, Y. De Vos, H.C.L. Abbenhuis, G. Gerritsen, A. J.J. Koekkoek, C. Cannilla, F. Fusteri, Effectiveness of the 3D-printing procedure in the synthesis of hybrid catalysts for the direct hydrogenation of CO2 into dimethyl ether, J. CO2 Util. 70 (2023) 102458.